Spatiotemporal dynamics of Raman coherence in hollow-core fibers for a pump-probe setup

Anton Husakou
Max Born Institute, Max Born Straße 2a, 12489 Berlin, Germany and GPPMM Group, Xlim Research Institute, CNRS, UMR No. 7252,University of Limoges, 87060 Limoges, France

Ying-Ying Wang, Meshaal Alharbi, and Fetah Benabid*
GPPMM Group, Xlim Research Institute, CNRS, UMR No. 7252, University of Limoges, 87060 Limoges, France

(Received 4 October 2017; published 9 February 2018)

We present an experimental and theoretical study of the stimulated Raman emission in hollow-core kagome waveguides in a pump-probe arrangement. We perform an experimental investigation of the power of the Stokes signal from the probe, which is below the stimulated Raman scattering threshold, as a function the pump-probe delay time. The results show the Stokes power to increase with pump-probe delay, reaching a maximum at 10 ns, and to decrease afterward. In view of a coherence decay time of only 0.25 ns, we demonstrate a surprisingly slow reduction of Stokes signal with the characteristic time much longer than the coherence decay time by a factor of up to 40. The numerical investigations explain the observed phenomenon as a result of the spatiotemporal dynamics of the probe pulse and Raman coherence. We show that the increase of the characteristic time can be related to the spatial position of the intense sideband generation event and its dependence on the pump-probe delay.

DOI: 10.1103/PhysRevA.97.023814

I. INTRODUCTION

The Raman effect has a long and successful history as a tool for time-resolved study of inorganic and organic molecules as well as biological tissue and for optical frequency conversion whereby it is used as a light source at wavelengths which are difficult to address with existing lasers. The application areas include time-resolved investigation of the chemical reactions, imaging of the subcell structure, detection of various substances, and so on (see, e.g., [1–3]), or the generation of ultrabroad radiation coherent sources for extremely short pulse synthesis [4–6]. Furthermore, because in Raman generation the Stokes light builds up from the quantum noise, the Raman effect has been used as a platform to explore quantum and coherent effects [7], such as the expansion of the initial Stokes field into statistically independent spatial coherence modes [8] and selection of one single coherent mode (i.e., pure quantum state) to be amplified to the macroscopic level while exhibiting nonclassical properties [9].

The invention of band-gap hollow-core photonic crystal fibers (HCPCFs) [10], which guide light due to the absence of the modes in the cladding, and kagome hollow-core fiber [11,12], with a guiding mechanism based on inhibited coupling to the modes in the cladding, opened new horizons in the studies of the Raman scattering and associated phenomena [11,13,14]. These new perspectives are facilitated by both strong light localization in a hollow core with a micrometer-scale radius and low transmission loss, allowing for significant propagation lengths and high values of the net gain G. Among the results of this previous work on stimulated Raman scattering (SRS) in gas-filled HCPCFs we note the SRS generation occurring in the transient regime even with pulses much larger than the dephasing time T_2 of the Raman resonance and the coherence properties of the lines initiated from vacuum fluctuations exhibiting surprisingly strong intrapulse self-coherence and mutual coherence [11]. The reason for this behavior is that the dephasing time becomes longer than the Stokes pulse duration for strong gain, since the Stokes pulse duration is inversely proportional to the net gain. This opens new prospects in a number of applications, such as generation of a coherent optical frequency comb, attosecond pulse generation, and optical waveform synthesis with pulse-to-pulse locking. Furthermore, in another work [15], using a delayed probe technique, we showed that the molecular coherence persists after duration as large as 42 times that of the dephasing time. While higher intensity and propagation lengths allow us to achieve unprecedentedly high Raman gain, they also allow for transient effects for relatively long pulses, raising questions about the spatiotemporal structure of coherence for propagation in hollow-core fibers. In order to be able to properly interpret the experimental results, it is therefore important to elucidate the effects which originate from spatial dynamics of the pump pulse, sideband pulses, and Raman coherence.

So far, the theoretical understanding of the processes which happen in the photonic crystal fibers has not been sufficiently developed. In particular, the spatiotemporal dynamics of the propagating pulse and of the Raman coherence is not fully understood. The analytical description can be developed only in the linear regime. However, the most efficient and useful research of Raman processes happens in the regime of strong excitation and coherence of the order of unity, in particular since the photonic crystal provides strong light intensity in

*f.benabid@xlim.fr

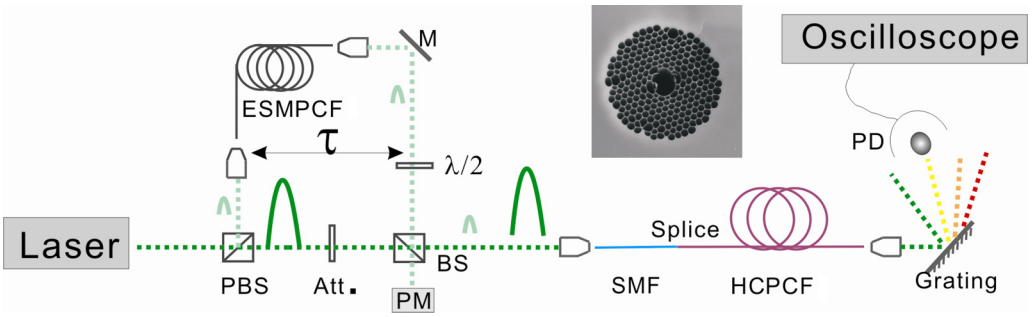

FIG. 1. Experimental setup for the molecular coherence measurement: ESMPCF, endlessly-single-mode photonic crystal fiber; PBS, polarization beam splitter; M, mirror; Att., attenuator; PM, power meter; BS, beam splitter; SMF, single-mode fiber; and PD, photodetector.

the interaction region. In this case, only a numerical treatment of such an inherently nonlinear problem is able to provide a proper understanding of the process and to explain the enigmatically slow decay of the Stokes signal versus pump-probe delay mentioned before. The dynamics of the coherence and its dependence on the propagation coordinate can strongly influence the Stokes intensity and its dependence on the pump-probe delay, as explained in several previous works (see, e.g., [16]). This study will be useful in understanding pulse to pulse Raman coherence generation and its findings can be applied in the fields of waveform synthesis and mode-locked lasers based on Raman excitation.

In this paper, we investigate experimentally and theoretically the dependence of the Stokes signal from a probe pulse on the delay between the pump and probe pulses which are sent in hydrogen-filled hollow-core photonic crystal fiber. We find that this dependence exhibits a maximum around 6 ns, with a subsequent slow decrease with a characteristic time of 10 ns, much longer than the coherence decay time, which is around 0.25 ns for the pressure of 20 bars considered here. Our numerical investigations allow us to explain this behavior and to prove that it is related to the event when the Stokes and anti-Stokes components are generated with high efficiency, in particular to the dependence of its spatial position on the delay. The numerical findings are in quantitative agreement with the experiment.

II. EXPERIMENTAL SETUP AND RESULTS

Figure 1 shows schematically the experimental setup. Here we use a delayed probe-pump technique whereby the Stokes generated by a weak pulse is monitored in the case of the absence and presence of a strong leading pulse. The two pulses, pump and probe, have the same wavelength of 532 nm and duration of 550 ps and are generated by the same source: a doubled Nd:YAG diode pumped solid-state microchip laser producing pulses with a 7-kHz repetition rate and an average output power up to 25 mW (peak power ∼6 kW). The delay between the two pulses is controlled by sending the probe pulse through a chosen length of endlessly-single-mode photonic crystal fibers. The average power of the probe beam is set at 0.4 mW, chosen so that the probe beam alone does not produce significant Raman excitation and sidebands generation in hydrogen-filled HCPCFs. Our estimates indicate that probe Raman gain is approximately 14, which is lower than the threshold value of roughly 20–25. The leading beam average power can be varied between 1 and 6 mW. Figure 1 also shows the scanning electron microscope image of the HCPCFs used here, which is a photonic band-gap guiding fiber with a transmission window ranging from 500 to 650 nm (∼140 THz) with an attenuation of 0.6 dB/m. The core of the fiber is not circularly symmetric; the dependence of the results on the pump polarization was not studied, however, we have optimized the input polarization to achieve maximum Stokes signal. The fiber has a core diameter of 5.4 μm, is 2 m long, and is filled with H_2 at a pressure of 20 bars. The output end of the fiber is attached to a gas chamber, while the input end is spliced to a single-mode fiber with a cutoff wavelength around 400 nm. This single-mode fiber acts as a seal for hydrogen-filled HCPCFs and as a spatial mode filter to provide exactly the same mode-coupling conditions for the two beams. The very small diameter of the HCPCFs provides an extremely large intensity even with very low laser power. For example, for the 6-mW average power provided by the pump pulse, the intensity that propagates inside the fiber is in excess of 10 GW/cm^2. With a constant laser intensity, the Stokes intensity grows with propagation coordinate z as $\exp(Gz/L)$, where G is the steady-state gain-length product (Raman net gain) and L is the fiber length. As a result, the Raman net gain $G = g_0 I_p L$, where g_0 is the Raman gain and I_p is the pump power, reaches ∼5000 for a length of fiber L of 2 m. At the HCPCF output, both the pump and probe Raman lines are separated with a grating and the first-order Stokes lines from both pulses are recorded. We note here parenthetically that, as will be shown later, the observed effects are mostly related to the propagation dynamics and therefore on the Raman gain, which does not strongly depend on pressure for the considered parameter range. Therefore, we do not expect a strong dependence of the results on the pressure, although systematic investigation was not performed.

The fiber transmission and typical output spectrum for the above-described setup are shown in Fig. 2. The transmission band extends from 480 to 590 nm, with transmission in the middle of the band very close to unity. The spectrum shown in Fig. 2 by the red curve features the pump at 533 nm; Stokes sidebands at 550, 567, 587, and 610 nm; an anti-Stokes sideband at 517 nm from the rotational Raman transition of the ortho-H_2; and weaker lines at 535 and 553 nm which originate from para-H_2. One can see that the transmission band, on one hand, is broad enough to include several sidebands; on the other hand, one does see that energy can be transferred to the spectral region with high loss, especially at high power and significant Raman excitation.

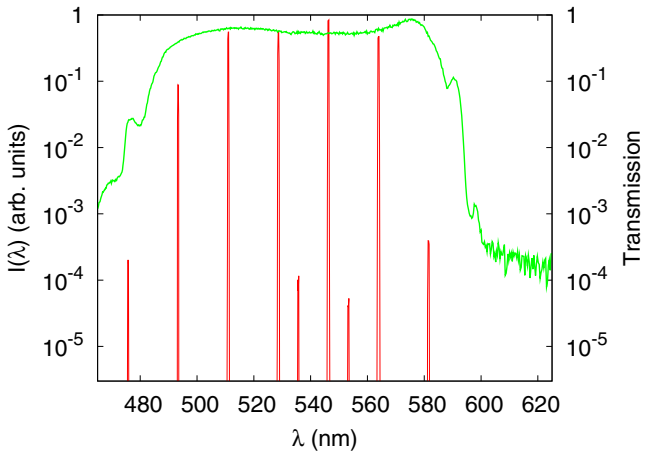

FIG. 2. Transmission of the fiber [green (upper) curve] and the output spectrum (vertical red lines). The spectrum is shown for a 0.55-ns pump pulse at 532 ns with an intensity of 14 GW/cm^2. The probe pulse is delayed by 3 ns; it has the same duration and wavelength as the pump pulse and an intensity of 35 MW/cm^2. The fiber has a radius of 2.7 μm and is filled with H_2 at a pressure of 20 bars at room temperature.

In Fig. 3(a), the dependence of the output Stokes signal on time is presented with and without a pump pulse in addition to the probe pulse. One can see that the probe pulse alone barely generates any significant Stokes signal, while the presence of the pump pulse before the probe pulse leads to a strong Stokes signal from both the pump and probe. This is explained by the Raman coherence which survives the delay between the pulse and triggers the generation of the Stokes signal from the probe.

The dependence of the Stokes signal of the probe pulse on the pump-probe delay is shown in Fig. 3(b). One can see the maximum of the signal at a delay of roughly 10 ns, as well as the decrease of the signal for a larger delay with a characteristic time in the range of tens of nanosecond. This time is much larger than the coherence decay time of 0.25 ns. This surprising contradiction will be explained in the next section by comprehensive numerical simulations.

III. THEORETICAL AND NUMERICAL APPROACH

To simulate the pulse propagation in the above-described setup, we rely on the forward Maxwell equations augmented by the Bloch equations for the density matrix. We assume that the coupling to higher-order transverse fiber modes is weak; therefore, the electric field in the waveguide can be presented in the form

$$\vec{E}(x,y,z,t) = \tfrac{1}{2}A(z,t - z/v_g)\vec{F}(x,y)e^{-i\omega_0 t}e^{i\beta(\omega_0)z} + \text{c.c.}, \tag{1}$$

where ω_0 is the central frequency, $\beta(\omega)$ is the frequency-dependent wave number of the eigenmode $\vec{F}(x,y)$, $v_g = [\partial\beta(\omega)/\partial\omega(\omega_0)]^{-1}$, and $A(z,t - z/v_g)$ is the complex envelope which characterizes the pulse. Note that all the Raman sidebands are represented by a single envelope. This allows for a much more compact and systematic description than the standard approach whereby each Raman sideband is characterized by its own envelope. As a trade-off, the grid step in time must be much less than the Raman period, increasing the numerical effort somewhat. We also assume that the total spectral width of the generated radiation stays below the central frequency due to the limited transmission band of the fiber.

The propagation equation for the Fourier transform of the envelope $A(z,\omega)$ has the form

$$\frac{\partial A}{\partial z} = -[\alpha(\omega+\omega_0) - i\beta(\omega+\omega_0) + i\beta(\omega_0) + \partial\beta/\partial\omega(\omega_0)(\omega-\omega_0)]A + \frac{i\omega_0}{2c\epsilon_0}P_{\text{nl}}(z,\omega), \tag{2}$$

where $\alpha(\omega)$ is the linear loss and the quantity $P_{\text{nl}}(z,\omega)$ is the Fourier transform of the nonlinear Raman polarization. For derivation and details regarding this equation, see, e.g., [17]. The nonlinear Raman polarization is defined in time domain as $P_{\text{nl}}(z,t) = N\,\text{tr}[\rho(z,t)\mu]A(z,t)$, where ρ is the dimensionless

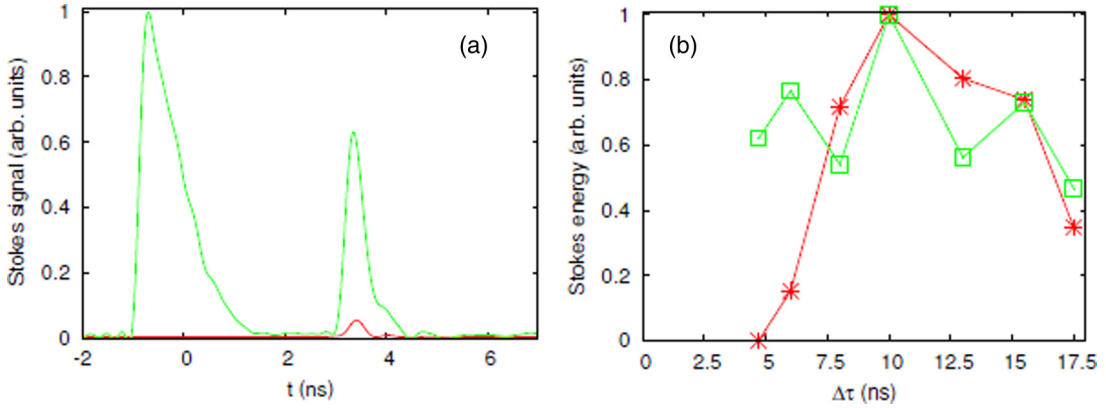

FIG. 3. (a) Output Stokes signal as a function of time excitation with only the probe signal [red (dark gray) curve exhibiting a small spike around 3.5 ns] and with the pump and probe signal [green (light gray) curve] and (b) the dependence of the Stokes signal (arbitrary units) of the probe pulse on the pump-probe delay. The wavelength and the duration of both pump and probe pulses is 532 nm and 0.55 ns correspondingly. Experimental data are depicted for pump intensities of 5 GW/cm^2 (red stars) and 14 GW/cm^2 (green squares). The peak probe pulse intensity is 35 MW/cm^2 and the propagation length is 4 m. A fiber with a radius of 2.7 μm filled with H_2 at a pressure of 20 bars at room temperature is considered.

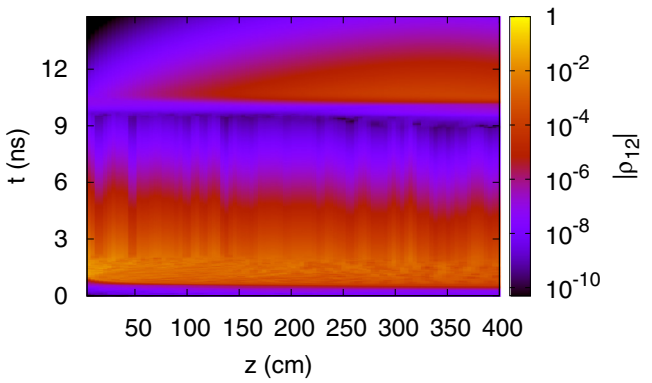

FIG. 4. Map of coherence $|\rho_{12}|$ as a function of propagation coordinate and time, for a delay of 8.88 ns. The pump pulse peak intensity is 42 GW/cm^2. The wavelength and the duration of both the pump and probe pulses are 532 nm and 0.55 ns, respectively. The propagation length is 4 m. A fiber with a radius of 2.7 μm filled with H_2 at a pressure of 20 bars at room temperature is considered. The pump pulse is centered at $t = 1.44$ ns and the probe pulse at $t = 10.32$ ns.

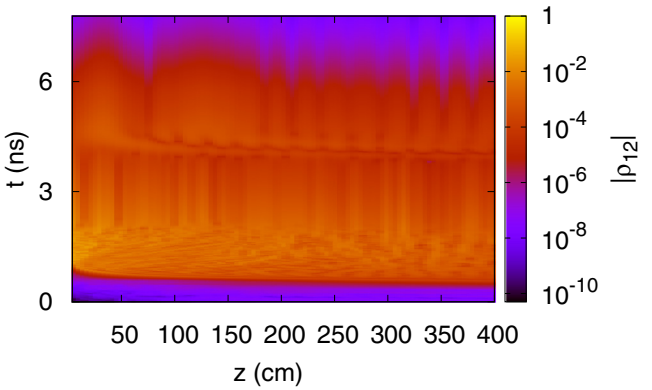

FIG. 5. Map of coherence $|\rho_{12}|$ as a function of propagation coordinate and time, for a delay of 2.88 ns. The pump pulse peak intensity is 42 GW/cm^2. The wavelength and the duration of both the pump and probe pulses are 532 nm and 0.55 ns, respectively. The propagation length is 4 m. A fiber with a radius of 2.7 μm filled with H_2 at a pressure of 20 bars at room temperature is considered. The pump pulse is centered at $t = 1.44$ ns and the probe pulse at $t = 4.32$ ns.

density matrix of the system, μ is the dipole moment matrix, and N is the particle density. The nonlinear properties of the system are determined by the temporal evolution of the $\rho_{12} = \rho_{21}^*$ and $\rho_{22} = 1 - \rho_{11}$ components of ρ, given by

$$\left(\frac{\partial}{\partial t} + \frac{1}{T_2} - i\Omega\right)\rho_{12} = \frac{i}{2\hbar}[(\alpha_{11} - \alpha_{22})\rho_{12} + \alpha_{12}\omega]|A|^2,$$
$$\left(\frac{\partial}{\partial t} + \frac{1}{T_1}\right)\rho_{11} = \frac{1}{T_1} - \frac{i\alpha_{12}}{4\hbar}(\rho_{12} - \rho_{12}^*)|A|^2, \qquad (3)$$

where Ω is the Raman frequency shift, T_1 and T_2 are the population and coherence decay times, respectively, and the α's are the Raman polarizabilities. For further details and the values of the coefficients used, see [18,19].

The above equations were solved by the split-step Fourier-transform method, accompanied by the second-order Euler method for the evolution of the density matrix. A grid resolution of 5.52 fs was used, which allows us to treat all the sidebands together and to resolve the oscillations of ρ_{12} which happen at the frequency corresponding to the Raman frequency shift. In the temporal ranges where the electric field is absent, such as between the pump and probe pulse, Eqs. (3) were solved analytically. The separation between the pump and probe pulses allowed us to calculate the z-dependent density matrix after the pump pulse once and use it for different delays, thus reducing the numerical effort.

IV. EXPERIMENTAL SETUP AND RESULTS

Before we proceed to the detailed explanation of the enigmatically large characteristic Raman signal decay time described in Sec. II, it is instructive to study the spatiotemporal maps of coherence, which are presented in Figs. 4 and 5 for two different pump-probe delays and with parameters corresponding to the experimental conditions and given in the captions. In both cases, the pump pulse produces a significant coherence already after a short propagation distance on the order of 1 cm. At that distance, a coherence of the order of unity is reached and simultaneously several Raman sidebands in the pump pulse spectrum (not shown) are excited with quantum efficiency close to unity. We call such an event high-efficiency Raman generation (HERG) for the pump pulse. For distances after the HERG event, the coherence for the pump pulse starts to drop, due to interference between the fields of the Raman sidebands. The temporal dependence of the coherence shows that after the pump pulse is over, the coherence decays exponentially in time, characterized by the T_2 decay time. Now let us turn to the probe pulse. The intensity of the probe pulse is sufficiently high so that it develops a certain coherence by itself by the Raman scattering of probe photons, just as it would happen in a strong enough single pump pulse, with maximum ρ_{12} values of up to 10^{-3}. This coherence buildup is enhanced by the leftover coherence of the pump pulse. In the case of large delay, illustrated by Fig. 4, however, the coherence of the pump pulse is reduced significantly when the probe pulse arrives. Therefore, the rise of coherence caused by the probe pulse is only slightly enhanced by the presence of the pump pulse and the HERG event does not occur for the larger 8.88-fs delay. The situation is different for the short 2.88-ns delay, as shown in Fig. 5. Due to the strong contribution of the pump coherence, the HERG event occurs already after a distance of 30 cm, and after that, the coherence oscillates with a decreasing tendency.

The above trends are additionally illustrated by the coherence as a function of time at the fiber output [Fig. 6(a)] and by coherence as a function of the propagation coordinate after the probe pulse [Fig. 6(b)]. In Fig. 6(a) one can see the coherence rise during the pump pulse, the consequent decay characterized by time T_2, and the coherence rise resulting from the probe pulse. Just after the middle of the pump pulse, the coherence reaches levels around 10^{-3} for both 2.88-ns and 8.88-ns delays, as can be seen in Fig. 6(a) at $t \sim 2$ ns, and starts to decay until the probe pulse arrives.

Note that even after the 8.88-ns delay, there remain roughly 5×10^7 molecules which still bear coherent excitation induced

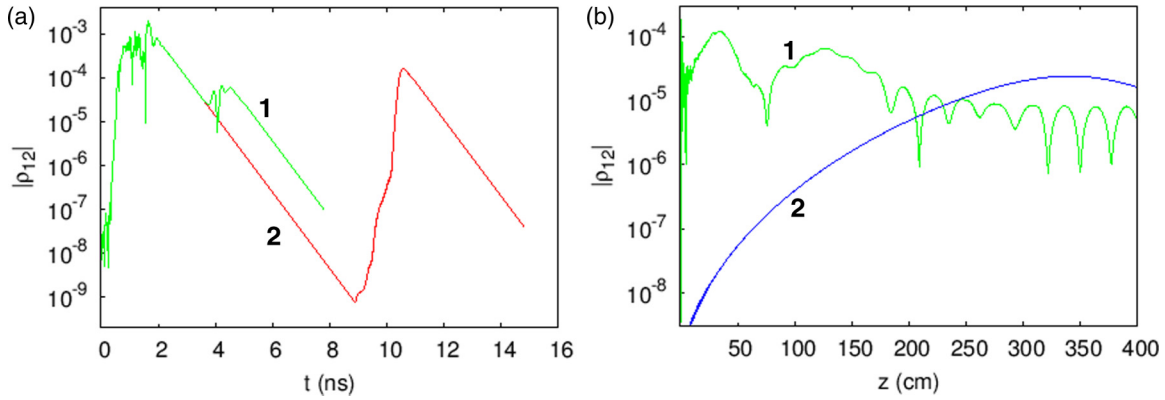

FIG. 6. Coherence $|\rho_{12}|$ (a) at the fiber output as a function of time for delays of 8.88 ns (red curve 2) and 2.88 ns (green curve 1) and (b) after the probe pulse as a function of propagation coordinate for delays 8.88 ns (blue curve 2) and 2.88 ns (green curve 1). The pump pulse peak intensity is 42 GW/cm^2. The wavelength and the duration of both the pump and probe pulses are 532 nm and 0.55 ns, respectively. The propagation length is 4 m. A fiber with a radius of 2.7 μm filled with H_2 at a pressure of 20 bars at room temperature is considered.

by the pump. This number is well above the threshold number of molecules of ∼200, calculated using the formalism of Ref. [16], which defines the border between coherent SRS and Raman excitation from noise. This means that for the configuration considered the Stokes buildup for the probe is based on the coherence left after the pump pulse and not on noise.

The qualitative difference in behavior for two delay times is more clearly visible for the coherence as a function of the propagation coordinate, shown in Fig. 6(b). One can clearly see that for a small delay, the HERG event at roughly 30 cm is followed by a decrease of the coherence with propagation distance, with a decrease of more than one order of magnitude over the propagation length. In contrast, for the longer delay, a steady increase of the coherence (except for a small section near the end of the fiber) is predicted.

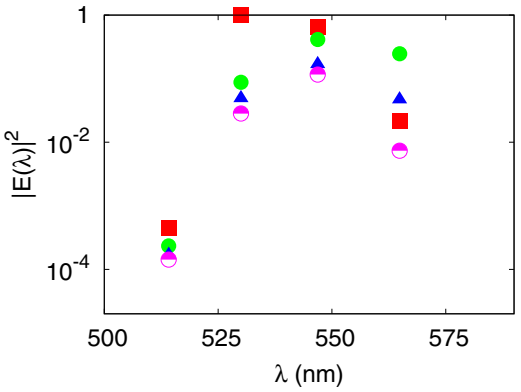

FIG. 7. Spectra of the probe pulse after 40 cm (red squares), 160 cm (green filled circles), 280 cm (blue triangles), and 400 cm (magenta half-filled circles) for a delay of 2.88 ns. The pump pulse peak intensity is 42 GW/cm^2. The wavelength and the duration of both the pump and probe pulses are 532 nm and 0.55 ns, respectively. The propagation length is 4 m. A fiber with a radius of 2.7 μm filled with H_2 at a pressure of 20 bars at room temperature is considered. For clarity, only the corresponding maxima of the spectral lines are presented; the lines themselves are too narrow to be resolved on this plot.

Let us now turn our attention to the spectra of the generated pulse. For the 2.88-ns delay the spectra of the probe pulse are depicted for propagation distances of 40, 160, 280, and 400 cm in Fig. 7. One can see that after the HERG event, the spectral lines cover the whole transmission band of the fiber, with some radiation emitted even outside the transmission band despite the loss of the fiber. The total energy in the fiber reduces with propagation, as can be seen from comparison of the red and magenta curves.

We are now in position to understand the characteristic time of the Raman signal decrease as depicted in Fig. 3. In Fig. 8, the dependence of the energy of the first Stokes sidebands versus the propagation distance is depicted for four different delays: 2.88, 4.88, 6.88, and 8.88 ns. One can see that for short delays, the HERG event for the probe pulse happens before the fiber end and the propagation after this event leads to decreased energy of the Stokes sideband due to loss outside the transmission band (see the red curve in Figs. 8 and 2). This

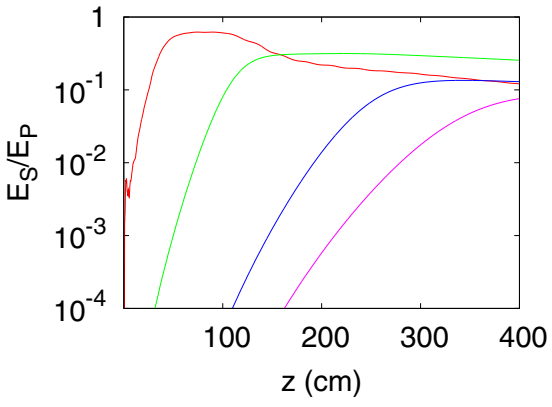

FIG. 8. Energy of the Stokes component of the probe pulse as a function of the propagation distance for delays of, from left to right, 2.88 ns (red curve), 4.88 ns (green curve), 6.88 ns (blue curve), and 8.88 ns (magenta curve). The pump pulse peak intensity is 42 GW/cm^2. The wavelength and the duration of both the pump and probe pulses are 532 nm and 0.55 ns, respectively. The propagation length is 4 m. A fiber with a radius of 2.7 μm filled with H_2 at a pressure of 20 bars at room temperature is considered.

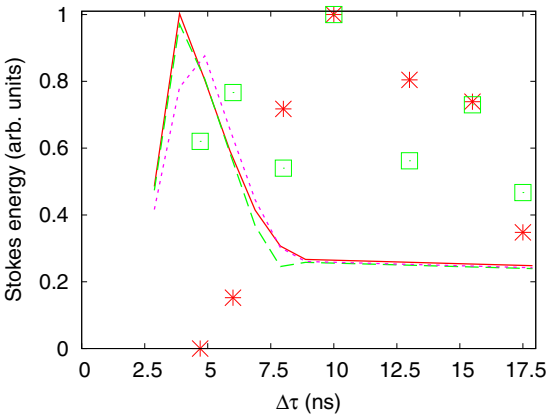

FIG. 9. Experimental and theoretical dependence of the Stokes signal (arbitrary units) of the probe pulse on the pump-probe delay. The wavelength and the duration of both the pump and probe pulses are 530 nm and 0.55 ns, respectively. Numerically calculated dependences are presented for pump pulse intensities of 5 GW/cm^2 (red solid curve), 14 GW/cm^2 (green dashed curve), and 42 GW/cm^2 (magenta short-dashed curve). Experimental data for pump intensities of 5 GW/cm^2 (red stars) and 5 GW/cm^2 (green squares) are repeated from Fig. 3. The peak probe pulse intensity is 35 MW/cm^2 and the propagation length is 4 m. A fiber with a radius of 2.7 μm filled with H_2 at a pressure of 20 bars at room temperature is considered.

explains the relatively low values of the Stokes energy for low delays visible in Fig. 3. With increasing delay it takes a longer propagation to reach the HERG event, which shifts towards the end of the fiber, with the maximum Stokes energy provided by HERG exactly at the fiber end (see the blue curve in Fig. 8). Finally, for even longer delays, the HERG is not reached (see the magenta curve in Fig. 8). The decreasing Stokes energy for longer pump-probe delays is explained by the decreasing contribution of the pump coherence to the stimulated Raman process in the probe pulse. We stress that there exists no linear relation between the coherence remained after the pump pulse and the Stokes energy under the conditions when the probe pulse can generate significant Raman coherence by itself, as it is the case under the conditions considered.

Thus, we explain the observed maximum followed by the slow decrease of the Stokes signal by a spatial shift of the position where the probe HERG event occurs and the disappearance of this event for longer delays. The predicted dependence of the Stokes component on the delay is shown in Fig. 9. There is a twofold discrepancy between the delay at which the maximum Stokes signal is achieved. However, this disagreement is quite acceptable in view of the complexity of the numerical simulations with many effects taken into account without any fit parameters or parameters adjustment. The discrepancy could be caused by, e.g., an inaccurate value of the decay time T_1, which is hard to access experimentally, as well as coupling losses which can influence reaching HERG. Despite the disagreement, the general form of the experimental dependence of the Stokes sideband on the delay is well reproduced by simulations.

V. CONCLUSION

An experimental and theoretical study of the stimulated Raman emission for the pump-probe arrangement was performed. We demonstrated a decrease of the Stokes signal with characteristic time much longer than the coherence decay time. To explain the observed phenomenon we used a comprehensive numerical model. This allowed us to relate the observed decay time to spatiotemporal dynamics of the probe pulse and Raman coherence. We explained the surprising increase of the characteristic decay time by analyzing the spatial position of the intense sideband generation event and its dependence on the pump-probe delay.

[1] Y.-C. Liu and R. L. McCreery, J. Am. Chem. Soc. **117**, 11254 (1995).
[2] K. Klein, A. M. Gigler, T. Aschenbrenner, R. Monetti, W. Bunk, F. Jamitzky, G. Morfill, R. W. Stark, and J. Schlegel, Biophys. J. **102**, 360 (2012).
[3] K. A. Misra, K. S. Sharma, T. E. Acosta, and J. N. Porter, Appl. Spectrosc. **66**, 1279 (2012).
[4] A. V. Sokolov, D. R. Walker, D. D. Yavuz, G. Y. Yin, and S. E. Harris, Phys. Rev. Lett. **85**, 562 (2000).
[5] F. Couny, F. Benabid, P. J. Roberts, P. S. Light, and M. G. Raymer, Science **318**, 1118 (2007).
[6] H.-S. Chan, Z.-M. Hsieh, W.-H. Liang, A. H. Kung, C.-K. Lee, C.-J. Lai, R.-P. Pan, and L.-H. Peng, Science **331**, 1165 (2011).
[7] M. G. Raymer and I. A. Walmsley, Prog. Opt. **28**, 181 (1990).
[8] M. G. Raymer, Z. W. Li, and I. A. Walmsley, Phys. Rev. Lett. **63**, 1586 (1989).
[9] I. A. Walmsley and M. G. Raymer, Phys. Rev. Lett. **50**, 962 (1983).
[10] P. S. J. Russel, J. Lightwave Technol. **24**, 4729 (2006).
[11] F. Benabid, J. C. Knight, G. Antonopoulos, and P. S. J. Russel, Science **298**, 399 (2002).
[12] F. Couny, F. Benabid, and P. S. Light, Opt. Lett. **31**, 3574 (2006).
[13] F. Benabid and J. Roberts, J. Mod. Opt. **58**, 87 (2011).
[14] Y. Y. Wang, C. Wu, F. Couny, M. G. Raymer, and F. Benabid, Phys. Rev. Lett. **105**, 123603 (2010).
[15] A. Husakou, Y. Y. Wang, B. J. Mangan, and F. Benabid, *2011 Conference on Lasers and Electro-Optics Europe and 12th European Quantum Electronics Conference (CLEO EUROPE/EQEC)* (IEEE, Piscataway, 2011).
[16] M. G. Raymer, I. A. Walmsley, J. Mostowski, and B. Sobolewska, Phys. Rev. A **32**, 332 (1985).
[17] A. V. Husakou and J. Herrmann, Phys. Rev. Lett. **87**, 203901 (2001).
[18] L. Meng, Ph.D. thesis, Montana State University, 2002.
[19] V. P. Kalosha and J. Herrmann, Phys. Rev. A **68**, 023812 (2003).